Version of Record: https://www.sciencedirect.com/science/article/pii/S0012821X21002880
Manuscript_a97dd6ab55b9c6f0fa952b35d499bf73

A hemispheric asymmetry in poleward ocean heat transport across climates: implications for overturning and polar warming☆

Emily Newsom[a], Andrew F. Thompson[b], Jess Adkins[b], Eric Galbraith[c]

[a]*Department of Physics, University of Oxford, UK*
[b]*Division of Geological and Planetary Sciences, Caltech, USA*
[c]*Earth and Planetary Science, McGill University, Canada*

Abstract

The modern Indo-Pacific oceans absorb more heat from the atmosphere than they release. The resulting energy surplus is exported from the Indo-Pacific by the ocean circulation and lost to the atmosphere from other ocean basins. This heat transport ultimately sustains much of the buoyancy lost to deep water formation at high latitudes, a key component of the global overturning circulation. Despite the fundamental link between inter-basin ocean heat transport and global overturning in today's climate, there is no general understanding of how these phenomena vary with climate state. Here, we use an unprecedented suite of fully-coupled climate model simulations, equilibrated for thousands of years to a wide range of CO_2 levels, to demonstrate that major differences in overturning between climates are related to systematic shifts in ocean heat transport between basins. Uniformly, equilibration to

☆Corresponding author
Email address: emily.newsom@physics.ox.ac.uk (Emily Newsom)

higher CO_2 levels strengthens inter-basin ocean heat transport and global deep water formation. These changes are sustained by increased surface heat uptake within the Indo-Pacific oceans, and increased high-latitude heat loss outside of the Indo-Pacific oceans as the climate warms. However, poleward heat transport and high-latitude heat loss do not increase symmetrically between hemispheres. Between glacial and modern-like states, North Atlantic heat loss intensifies and overturning in the Atlantic strengthens. In contrast, between modern-like and hot climates, heat loss and overturning strengthens in the Southern Ocean. We propose that these differences are linked to a shift in the relative efficiency of northward and southward ocean heat transport — dominated by advection in the North Atlantic and eddy diffusion in the Southern Ocean — with climate state. Our results suggest that, under high CO_2, future ocean heat transport towards Antarctica would increase disproportionately compared to its changes since the last ice age.
Keywords: Paleoclimate, Climate Evolution, Ocean Overturning Circulation, Ocean Heat Transport, Climate Modeling, Last Glacial Maximum

1. Introduction

In the modern climate, the combined heat transport by the ocean and atmosphere alleviates the energy imbalance between the planet's low and high latitudes. While the atmosphere extends over the entire Earth surface, the global ocean is instead partitioned by continents into basins. Each basin differs dramatically in shape and meridional extent, such that the Indian and Pacific Oceans make up most of the tropical global ocean, while the Atlantic, Arctic, and Southern Oceans comprise its high latitudes. Given this configuration, the surface heat budgets of each basin need not close. Instead, imbalances in surface heat fluxes over each basin are compensated by zonal heat transport between basins, accomplished through an inter-basin circulation (e.g., 1).

In the modern ocean, vast quantities of heat are carried between basins by the ocean circulation. Specifically, an excess of nearly a petawatt of heat is gained over the surface of the Indo-Pacific Oceans, which is relieved by a net heat transport into both the Southern and Atlantic Oceans (e.g., 2). This imported heat balances the net surface heat loss from these basins and plays a pivotal role in maintaining the modern deep Atlantic Meridional Overturning Circulation (AMOC) (1, 3, 4, 5, 6, 7). However, the strength and configuration of the ocean overturning has varied from its present-day state over past glacial cycles, as documented in deep ocean tracers and fluctuations in both atmospheric CO_2 and global surface temperatures (8, 9, 10). For instance, paleo proxies suggest that the AMOC was shallower and involved less inter-basin flow during the Last Glacial Maximum (LGM) than its present-day counterpart (e.g., 11, 12, 13). A comprehensive explanation for these changes remains elusive.

Despite the link between inter-basin ocean heat transport and the overturning circulation in the present-day climate, as well as the consensus that overturning has varied significantly in the past, no previous study has explored how changes in overturning are more generally connected to modifications in basin-scale surface heating and inter-basin ocean heat transport. Moreover, many prevailing dynamical theories for overturning transitions rely heavily on idealized ocean-only models (14, 15, 16, 17, 18, 19), frameworks that, by construction, do not account for the complex atmosphere-ocean dynamics that govern the geographical distribution of surface heat fluxes in a given climate.

In this study, we use an unprecedented ensemble of fully-coupled climate model simulations to show that the global distribution of surface heat fluxes, and compensating pathways of inter-basin ocean heat transport, vary systematically across a range of equilibrated climate states. Specifically, we find that, while the Indo-Pacific basins are always sites of net heat uptake, with a magnitude that increases with climate warming, the delivery of heat to sites of high latitude heat loss varies asymmetrically between the North Atlantic and Southern Ocean. We argue that this shifting distribution of global ocean heat loss explains global overturning reconfigurations exhibited across climates, which are qualitatively consistent with accepted differences between the overturning during the LGM and today. In addition, our results inform how past overturning transitions may differ from those possible in climates much warmer than today.

Climate Simulations and Methods

The relationship between the equilibrated ocean overturning state and global climate has remained unclear, in part, because of the computational challenges of addressing this relationship in climate models. Doing so inherently requires: (1) coupling of a dynamic ocean, atmosphere and crysophere; (2) a large number of simulations that probe different forcing and climate states; and (3) integrations that span many thousands of years to achieve a statistically-steady system (e.g., 20). Here, we make use of an unprecedented ensemble of simulations that satisfy these requirements. This series of 24 fully-coupled climate simulations, each equilibrated to a wide range of different atmospheric carbon dioxide (CO_2) levels under various orbital forcing scenarios, and individually integrated for at least 3000 years, comprehensively span quasi-equilibrium climate states from cold, glacial-like conditions, through modern-day parallels, and into states much warmer than today (21).

The climate model used is the coupled ocean− atmosphere−ice− biogeochemistry model CM2Mc.v2 (22) with a nominal 3° horizontal resolution in the ocean and in the atmosphere, each comprised of 28 and 24 vertical layers, respectively, as detailed in (21). The model was forced with one of six levels of atmospheric CO_2: 180, 220, 270, 405, 607 and 911 ppm. For each CO_2 level, the simulation was integrated using one of four different permutations of orbital forcing, involving two precession angles (270° or 90°) and two obliquities (22.0° or 24.5°), over timescales ranging from 3200 to 5000 years. The model set-up and the influence of orbital variations are discussed in depth by (21). To isolate the robust influence of CO_2 level on equilibrium climate, in this study we present averages at each atmospheric CO_2 level across the 4 orbital configurations. The general evolution of climate and ocean overturning with CO_2 level, averaged over the various orbital forcing scenarios, (summarized in Fig. 1a-d) are robust across each individual orbital forcing case. Fig. S1 expands on the characteristics of the overturning and climate state for different CO_2 forcing and orbital configurations, the spread of which is illustrated in the vertical bars in Fig. 1. Interesting differences do exist between different orbital configurations and will be explored in a subsequent study.

Our particular focus here is the influence of CO_2 level on global overturning and heat transport. We define the global overturning streamfunction from the residual circulation along and across density surfaces, given by

$$\Psi(y, \sigma) \equiv - \int_{-H}^{\zeta} \int_{x_E}^{x_W} \mathbf{v}(x, y, z) \mathcal{H}(\sigma'(\boldsymbol{x}) - \sigma) \, \mathrm{d}x \, \mathrm{d}z. \tag{1}$$

Eq. 1 quantifies the meridional transport of waters denser than isopycnal σ, where $\mathbf{v}(x, y, z)$ is the local residual meridional velocity (including bolus contributions), H is the depth of the ocean bottom, ζ the sea-surface height, $\mathcal{H}$ is the Heaviside Function, where $\mathcal{H}(n) = 1$ for $n \geq 0$ and $\mathcal{H}(n) = 0$ for $n < 0$, X_E and X_W are zonal boundaries of the domain, which can span a closed basin or a full longitude circle, and y is latitude. To exclude the surface gyres, the Atantic Meridional Overturning Circulation (AMOC) strength is defined as the maximum in Ψ within the Atlantic basin for all $\sigma > 34$ kg/m^3. Global abyssal overturning strength is defined as the minimum in Ψ for all $\sigma > 34$ kg/m^3 and north of 30°S, which captures the global overturning of the bottom waters destroyed through buoyancy gains north of 30°S. Total global overturning (Fig. 1c) is defined as the sum of the absolute magnitude of each overturning branch, quantifying the net global cycling of waters from high to low densities (and, generally, from lower to higher temperatures). Note that the maximum in the abyssal branch south of 30°S, or the "Southern Ocean recirculation" (e.g. 23), follows a trajectory distinct from the "global" value. This relationship, closely linked to Antarctic sea ice, and orbital forcing, will be explored in a subsequent study.

An key point is that the overturning rates we report are equilibrated to each CO_2 level and, in general, will differ from the ocean's transient response to changes in CO_2 forcing between states. While we have not performed a 20th-21st century simulation in this version of the model, we note the AMOC weakens in its transient response to historical and RCP8.5 forcing in two very similar model configurations (CM2M.v1 by (24) and GFDL ESM2M (25)), consistent with most coupled climate models. In contrast, several studies have shown that the AMOC ultimately recovers or exceeds its preindustrial strength as the climate equilibrates (over millennial timescales) to higher than present day CO_2 levels (20, 26, 27). This AMOC strengthening is in broad agreement with our simulations.

Several limitations of the simulations relevant to global overturning should be noted. Due to its coarse resolution, the ocean model does not resolve geostrophic turbulence and therefore parameterizes the effect of mesoscale eddies. Lateral diffusion and skew diffusion of tracers along isopycnals is represented using the parameterization of (28) with a spatially-varying diffusion coefficient. The coefficient depends on the horizontal shear between 100 and 2000 m, and is bounded by minimum and maximum values of 200 m^2 s^{-1} and 1400 m^2 s^{-1}, respectively. Overall, CM2Mc generates a relatively strong response to changes in baroclinicity, as suggested by observations in the Southern Ocean (29). The parameterization is an imperfect surrogate for eddy effects, and will therefore bias the results to some degree. Note, however, most of the large-scale aspects of interest here are captured relatively well by similar parameterizations (30). Additionally, like most global climate models, CM2Mc cannot capture the many processes involved in the coastal formation and overflow of deep waters, resulting in the dominance of bottom water formation through open-ocean convection. This likely biases the sensitivity of deep water formation to CO_2 change to some degree. More details of these limitations are discussed by (21). Of particular importance for our results is a cold bias in the North Pacific in its preindustrial control simulation, associated with more expansive sea ice and more vigorous intermediate water formation than observed in the region in the modern climate. In contrast, the Southern Ocean is warmer in preindustrial simulations than observed, though its preindustrial sea ice extent agrees relatively well with observations and quite well with CMIP5 and CMIP6 models, on average (31).

Finally, there is a small imbalance in the net surface heat flux, which when summed globally ranges from $0.01 - 0.06$ PW across climate states (Fig. S2), remaining $1 - 2$ orders of magnitude smaller than both net inter-basin heat transports and changes in inter-basin heat transport across climates. Regardless, deep ocean temperatures remain quite steady, changing less than 0.001°C on average over the final century of integration. We consider the potential impact of these model biases on our results in our Discussion.

Results

As expected, climate simulations equilibrated to progressively higher CO_2 levels warm monotonically, as measured by the atmospheric global mean surface temperature (GMST) (see 21). Warming of the climate state, in these simulations, also leads to major reconfigurations in inter-basin ocean heat transport, as we discuss in detail in the following sections. Changes in inter-basin transport can first be inferred by comparing the net heat flux over each basin (Fig. 1a-b). Across all climate states, the Indo-Pacific serves as the global ocean's primary heat source. This basin, defined as the region between 30°S and the Bering Strait in the Pacific and Indian Oceans, receives more heat from the atmosphere than it loses, meaning the Indo-Pacific surface heat flux is in surplus (is positive in the net, see Fig. 1a), irrespective of the climate state. Furthermore, this Indo-Pacific heat surplus grows monotonically with GMST, which, as a consequence, requires more heat to be exported from the basin in progressively warmer climates. However, the partitioning of heat loss to the atmosphere between the Atlantic-Arctic region (north of 30°S and including the marginal seas, henceforth "Atlantic") and the Southern Ocean (south of 30°S) follows a complex trajectory with increasing GMST (Fig. 1b).

The global overturning rate is tightly linked to basin-scale heating. Individually, the Atlantic-sourced (AMOC) and Southern Ocean-sourced (abyssal cell) branches of the global circulation tigtly co-vary with the total heat fluxes in their respective basin (Fig. 1d). Yet the combined magnitudes of each branch, which we term the global overturning rate, increases monotonically with the increasing Indo-Pacific heat uptake (Fig. 1c). We are not aware of prior discussion regarding this general relationship between the global overturning rate and global mean temperature — it would, in fact, be impossible to recover in a model that imposes surface fluxes or temperatures in the lower latitudes (15, e.g.,). In what follows,we refer to three distinct overturning states spanned by these simulations, termed "Cold" (low CO_2 at 180 ppm), "Warm" (near modern-day, at 405 ppm) and "Hot" (high CO_2, at 905 ppm), which differ in both the relative importance of the Atlantic and Southern Oceans in closing the global ocean heat budget and the relative contribution of the AMOC and abyssal cells to global overturning. Due to the equilibrated nature of the simulations, we cannot assess the transient adjustment that produces these changes in overturning, but we can determine the processes that sustain distinct configurations between climates. We first describe these key dynamical differences and then propose an explanation for why the circulation transitions between regimes.

Indo-Pacific Heat Uptake

We begin with the mechanisms sustaining the Indo-Pacific net heat surplus and its remarkably monotonic relationship with GMST. Across all climate states, most of the heat uptake in the basin (and globally) occurs in the tropical Pacific (here defined from 10°S to 10°N in the Pacific, (the red box in Fig. 2a). Tropical heat uptake exceeds total heat losses elsewhere in the basin in all climates (leading to the surplus in Fig. 1a). Moreover, heat uptake in the tropical Pacific, where wind-driven upwelling exposes cooler underlying waters to intense shortwave radiation, is relatively consistent between climates, decreasing by roughly 10% from 1.8 PW in the Cold state to 1.6 PW in the Hot state (Fig. 2b). In contrast, surface fluxes over the basin's dominant heat loss site — the North Pacific, defined as $12 - 55$°N (the blue box in Fig. 2b) — varies more significantly with climate. In the Cold state, 1.38 PW of heat is lost over this region (a net flux of -1.38 PW), whereas in the Hot state, regional heat loss falls 34% to -0.91 PW (Fig. 2b). This reduction is due to a weaker sensible heat loss. In fact, North Pacific sensible heat loss weakens more dramatically than the total heat loss, decreasing nearly two-fold from -1.53 PW to -0.85 PW between the Cold and Hot states (Fig. 2b). While sensible heat fluxes dominate total regional reductions, they are slightly offset by other flux components.

We attribute the change in sensible heat loss to a reduction in the air-sea temperature contrast (a primary control on sensible heat loss) over the North Pacific. In the glacial-like Cold state, regional surface air temperatures are 3.3°C colder, on average, than the sea surface below (i.e., an air-sea contrast of −3.3°C in Fig. 2c). As GMST increases, however, regional surface air temperatures warm more than sea-surface temperatures. This likely occurs because surface waters carried northward in western boundary currents acquire their characteristic temperatures from lower latitudes, where surface warming varies less with climate state. In contrast, North Pacific surface air temperatures are more sensitive to continental effects (e.g., 32)) and are influenced by the disproportionate warming of the land surface, relative to the ocean, between climates (e.g., 33, 34). This reasoning suggests that reductions in mid-latitude sensible heat loss may be a general expectation of a warming climate, an inference supported by the robust, wide-spread reduction in North Pacific and mid-latitude sensible heat loss in 20th and 21st century warming scenarios in the CMIP5 ensemble (35). While the comparison of these transient simulations to our results is indirect, we are not aware of any study examining the equilibrated regional heat flux response to CO_2 changes in other models. In our simulations, changes in regional surface climate significantly reduce the air-sea temperature contrast (to −1.6°C) in the North Pacific in the Hot state, consistent with the strong reduction in sensible heat flux between the climate states (Fig. 2c). While the magnitude of this heat loss may be influenced by the regional cold bias noted under preindustrial forcing (21), we argue that the qualitative change between climate states is not. That is, because North Pacific heat loss is more sensitive to climate state than tropical Pacific heat uptake, the basin-scale Indo-Pacific surface heat budget falls increasingly out of balance with increasing GMST.

Atlantic and Southern Ocean Heat Loss

To understand the (non-monotonic) evolution of basin-scale heat loss in the Atlantic and Southern Oceans (Fig. 1b,d), we first consider the dynamics that govern lateral heat transport. In the glacial-like Cold climate state, polar regions are extensively ice covered and global high-latitude heat loss is at its minimum (Fig. 2a and S3). In the Atlantic, the AMOC, which even in this climate is sustained by heat loss (Fig. 3), is relatively weak (at 15 Sv) and shallow (Fig. S6). Note that Fig. 3 depicts the surface water-mass transformation (e.g., Walin (36), and defined in Appendix A), which quantifies the relative roles of heat and freshwater fluxes in dense water formation.

The glacial AMOC is shallow and largely confined to the Atlantic basin, weakening to 8 Sv at 30°S, and there is a negligible heat transport into the basin (Fig. 1, S4). This implies that the AMOC is maintained by heat gained over lower latitudes within the Atlantic basin, consistent with the inference of reduced intermediate water inflow during past weak AMOC states (37). These features also generally agree with evidence of a shallower AMOC during the LGM, relative to present day (e.g., 8, 9, 10, 11). Previous analysis of CM2Mc has shown that the presence of a large Laurentide ice sheet intensifies local dense water formation and overturning rates within the shallow AMOC (21), but this effect is not included here. Deep and bottom water formation in the Southern Ocean, in contrast to the North Atlantic, is primarily sustained by vigorous brine rejection from Antarctic sea ice (Fig. 3 and (21)). This behavior again conforms to proxy-based reconstructions of a salinity-driven glacial abyssal overturning (38, 39). Thus in both the Atlantic and Southern Ocean in these simulations, Cold state overturning is qualitatively consistent with paleoclimate records and does not rely on net heat transport into the basin.

In warmer climates, global surface heat flux patterns shift, with important implications for deep overturning. As noted above, increasing Indo-Pacific heat uptake must be compensated by intensified heat loss elsewhere. Between the Cold and Warm states, the intensified cooling rates occur almost exclusively within the North Atlantic. North of 50°N, heat loss from a now ice-free surface more than doubles, from -0.22 PW to -0.47 PW, and accounts entirely for the nearly two-fold increase in deep water formation (Fig. 3) and AMOC strength (Fig. 1d). The enhanced AMOC is deeper and is no longer maintained by heat sourced within the Atlantic basin, but instead relies on a significant zonal heat transport (Fig. S4) from the Indo-Pacific and into the Atlantic along the canonical "warm route" (40). An increase in inter-basin circulation and heat transport with climate warming is also inferred from reconstructions (16) and is consistent with the strengthening and southward extension of Southern Hemisphere westerly wind stress (Fig. S8 and e.g., (41, 42)), also expected in warmer climates (e.g., 43). Stronger and deeper heat and buoyancy transport out of the Indo-Pacific and into the Atlantic (Fig. S6) is also a signature of inter-basin overturning (e.g., 6, 7), and is more consistent with the modern state (e.g., 5). In contrast to the North Atlantic, high-latitude heat loss in the Southern Ocean ($> 60°S$) remains largely unchanged between Cold and Warm states. Deep water formation and abyssal overturning rates weaken moderately, though this is primarily due to reduced Antarctic sea ice formation (Fig. 3), consistent with the $\approx 26\%$ decline in sea ice area. Further, Antarctic sea ice changes between the Cold and Warm state are small, relative to the precipitous reduction (by $\approx 84\%$) in Northern Atlantic ice area (Fig. 4a). Heat loss outside the Antarctic ice pack weakens, part of a robust global reduction in mid-latitude sensible heat loss (Fig. S3 and consistent with (35)).

While the transition between the Warm and Hot states is again characterized by increased inter-basin heat transport, in contrast to the Cold-to-Warm transition, North Atlantic heat transport and AMOC strength are nearly unchanged (Figs. 1, 3). Westerly winds remain sufficiently southward to enable exchange between the Indo-Pacific and Atlantic, yet heat transport along this pathway, as well as North Atlantic cooling rates, saturate at their Warm state levels (Figs. 4a, S4). Instead, increased Indo-Pacific heat uptake is compensated in the Southern Ocean. Specifically, southern high-latitude (> 60°S) cooling increases from -0.33 PW in the Warm state to its peak across all climates, -0.42 PW, in the Hot state. Additionally, Antarctic sea ice, relatively resilient to moderate changes in GMST, declines dramatically (Fig. 4a), even while bottom water formation and abyssal overturning reach their highest rates across all climate states. Notably, similar increases in AABW formation and abyssal overturning, concurrent with severe reductions in Antarctic sea-ice, were noted in climates equilibrated to above-present day CO_2 levels in other models (44, 45).

Crucially, this increased overturning is now maintained by intensified surface heat loss (Fig. 3), representing a systematic shift from an abyssal circulation driven by brine rejection in the Cold state to an exclusively heat-driven overturning in the Hot state. Enhanced meridional heat transport across the ACC balances surface flux changes (Fig. 4a). These changes are likely enabled by a southward shift of the ACC, resulting in its intensified interaction with topography and, thus, the formation of standing meanders (Fig. S4). Standing meanders are known sites of increased eddy activity and eddy fluxes (46, 47); indeed southward eddy heat fluxes increase nearly two-fold between the Warm and Hot states (Fig. S5). Deeper penetration of heat (and buoyancy) into the abyssal Indo-Pacific further implies enhanced coupling between low-latitude surface fluxes and global abyssal overturning (Fig. S6). Despite key differences in the Cold-to-Warm overturning reconfiguration versus the Warm-to-Hot, both are characterized by increased deep water formation driven primarily by increasing surface heat loss in the presence of declining sea ice (Fig. 3).

Climate-state Dependence of Poleward Heat Transport

Climate warming in these simulations is characterized by intensified heat transport from the tropics and towards the high latitudes. Yet, the partitioning of heat transport to the North Atlantic and Southern Ocean differs systematically across climates (Fig 4a). These differences are highlighted by the ratio

$$R_h \equiv \left(\frac{\Delta F_h^{\mathrm{NA}}}{\Delta F_h^{\mathrm{SO}}} \right), \tag{2}$$

where R_h captures the relative change in heat transport into the high latitudes of the North Atlantic (ΔF_h^{NA}) versus the Southern Ocean (ΔF_h^{SO}) between each climate. For $R_h > 1$ — a "Northern Receiving" regime — increases in North Atlantic heat transport exceed increases in heat transport across the Southern Ocean. For $R_h < 1$ — a "Southern Receiving" regime – the Southern Ocean is favored. R_h, diagnosed from the model output (Fig. 4b), indicates that the Warm state marks a transition from Northern Receiving between the coldest climates simulated ($R_h \approx 11$) to Southern Receiving ($R_h \approx 0.001$) between the warmest.

We propose that this evolution in R_h may be linked to how efficiently an adjustment in ocean dynamics can enable poleward heat transport in the North Atlantic and Southern Ocean. Qualitatively, this argument is based on the idea that heat transport by the AMOC depends sensitively on the meridional temperature gradients it acts across, gradients that may differ significantly between climates. In general, meridional heat transport F_h can have both mean and eddy contributions: $F_h \propto \overline{vT} = \left(\overline{v}\overline{T} + \overline{v'T'}\right)$, where $\overline{(\ )}$ and $(\ )'$ represent a zonal and temporal mean, and deviations from this mean, respectively. North Atlantic heat transport is largely advective, such that $\overline{vT} \approx \overline{v}\overline{T}$ (e.g., 48), and the heat transport scales as $F_h^{\mathrm{NA}} \sim \Psi \Delta T^{\mathrm{NA}}$. Here, Ψ, a volume transport, represents the AMOC strength, and ΔT^{NA} is the temperature difference between the subtropical and sub-polar Atlantic (as detailed in Appendix B). Heat transport across the zonally-unbounded Southern Ocean, on the other hand, depends on the efficiency of mixing and transport by mesoscale eddies (49), such that $\overline{vT} \approx \overline{v'T'}$, and the Southern Ocean heat transport scales as $F_h^{\mathrm{SO}} \sim WHK\Delta T^{\mathrm{SO}}/\ell$. Here W and H are the zonal and vertical extent of the ACC, K is a turbulent eddy diffusivity, and ΔT^{SO} and ℓ are the characteristic temperature difference and length scale across the ACC frontal zone, respectively (Appendix B).

Critically, the magnitudes of both F_h^{SO} and F_h^{NA} depend on aspects of the background climate state. This dependence also means that an equivalent perturbation to ocean dynamics in either region (i.e., $\delta\Psi$ or $\delta\ell$) will modulate meridional heat transport differently in different climates.

To isolate this effect, we calculate linear perturbations to F_h^{NA} and F_h^{SO}, i.e., δF_h^{NA} δF_h^{SO}, about each climate state and keep only terms containing dynamical perturbations (see Appendix B). Doing so assumes temperature differences ΔT^{NA} and ΔT^{SO} are representative features of the mean climate state. Here we assume K is constant across climate states, while acknowledging that previous studies have shown that K may vary with surface wind stress in the Southern Ocean (50). Uncertainty in K is incorporated in our estimate of $\delta\ell$. Combining these scalings,

$$R_h \approx \left(\frac{\delta F_h^{\mathrm{NA}}}{\delta F_h^{\mathrm{SO}}}\right) \sim R_e \left(\frac{\delta\Psi}{K\delta\ell}\right), \tag{3}$$

$$R_e \equiv \left(\frac{\Delta T^{\mathrm{NA}}}{\Delta T^{\mathrm{SO}}}\frac{\ell^2}{WH}\right). \tag{4}$$

Here, R_e describes how efficiently a perturbation in AMOC strength ($\delta\Psi$), relative to an equivalent contraction of the frontal zone in the ACC ($\delta\ell$, and scaled by K), would sustain increased heat transport to the high latitudes in a given climate. By this argument, the magnitude of R_e predicts whether climate warming will dynamically favor increased heat transport into the North Atlantic ("Northern Receiving", $R_e > 1$) or into the Southern Ocean ("Southern Receiving", $R_e < 1$), assuming that ocean dynamics (i.e., the scaling relationships for F_h^{NA} and F_h^{SO}) modulate this evolution. Note that R_e does not predict the total magnitude of the increased heat transport, which will also depends on changes to Ψ and ℓ (the last term in Eq. 2). Instead, R_e depends only on properties of the mean climate state, which we propose should precondition the efficiency of dynamic perturbations.

Fig. 4e illustrates that R_e is indeed prognostic of heat transport adjustments between each climate (although R_e does not scale with R_h alone). Like R_h, R_e falls sharply across simulations, primarily because ΔT^{NA} weakens with GMST (and the loss of North Atlantic sea ice, Fig. 4c, 5a, and S8), while ΔT^{SO} strengthens (Fig. 4c) as subtropical waters warm more than those around Antarctica (Fig. S7). As a result, $\Delta T^{\mathrm{NA}}/\Delta T^{\mathrm{SO}}$ falls roughly five-fold across the simulations (Fig. 4d). Additionally, ℓ contracts in warmer climates (Fig. 4d and S8) with the formation of more vigorous standing meanders in, and thus sharper fronts across, the ACC as discussed above (Fig. S5). In summary, characteristics of a cold climate result in $R_e \gg 1$ (Fig. 4e), suggesting that heat transport increases dynamically favor an adjustment of the AMOC (increasing $\delta\Psi$). Characteristics of warmer climates, however, hamper the efficiency of the northern mode of heat transport (i.e., R_e plummets to $R_e \approx 0.9 < 1$ in the Hot state); heat transport towards the Southern Ocean becomes a more viable pathway. The evolution of R_e is consistent with the systematic differences in the transitions between the Cold and Warm versus the Warm and Hot states (Fig. 1b, 4a-b). A key implication of this evolution, in the context of these simulations, is that the adjustment of ocean heat transport and overturning to forcing perturbations is climate-state dependent.

Discussion and Conclusions

While these simulations display complex changes in the global overturning between different climates, we draw attention here to several robust emergent features that suggest a new, relatively simple understanding. Across all states, climate warming involves a progressive poleward shift in the primary sites of global surface heat loss, met with reduced mid-latitude (primarily sensible) heat loss (Fig. S3). This poleward migration of heat loss impacts the total surface heat flux, summed over each basin, and is accompanied by enhanced heat redistribution between basins. This increased inter-basin coupling is linked to stronger cooling-driven deep-water formation (Fig. 3) and the incorporation of increasingly deep components of the ocean's overturning circulation in global heat transport (Fig. S7). The magnitude of these adjustments are phased differently in each hemisphere in a way that is consistently linked to key features of the background climate state (i.e., Eq. 4). Examined in isolation, these changes have a complicated relationship with GMST. Yet consideration of both hemispheres together shows that global overturning changes across all climates balance the magnitude of excess energy gained over the disproportionately tropical Indo-Pacific oceans.

The dynamics governing these changes in oceanic heat uptake and transport depend on fundamental properties of the climate and are thus likely to be robust across models. Yet, some limitations of our model may influence details of our results. For instance, a cold bias in the model's preindustrial North Pacific (21) could potentially impact the sensitivity of regional heat loss to CO_2 changes. Additionally, ours (and most) climate models cannot resolve the localized processes involved in deep-water formation. Yet several lines of evidence suggest that these biases don't underpin the qualitative evolution we describe. First, paleo-proxies suggest stronger North Pacific Intermediate Water formation during the (colder) LGM, while North Pacific sensible heat loss robustly weakens under 21st century (warming) scenarios in CMIP5 models (35). The consistency of these studies with ours may stem from the driving role of continentally-sourced westerlies in mid-latitude sensible heat loss (e.g., 32, 51), coupled with amplification of warming over land, relative to ocean, under CO_2 forcing (e.g., 33, 34). They imply that a reduction in the (disproportionately tropical) Pacific basin's ability to close its heat budget locally may be a basic feature of climate warming, which we leave for interrogation in other models. Secondly, the global overturning behaviors discussed here are qualitatively consistent with multiple inferred changes since the LGM, including the deepening of the AMOC (e.g., 8, 9, 10, 11), the reduced role of sea-ice in the AABW formation (e.g., 38, 39, 21, 12), and increasingly inter-basin global overturning (e.g., 16, 17, 13, 37). Overturning in the warmer states we describe is also consistent with the millennial-scale response to above present-day CO_2 forcing in other climate models, specifically the recovery or strengthening of the AMOC (20, 26, 27, 52) and the intensification of AABW production despite the near or total disappearance of Antarctic sea ice (27, 45). In sum, while our simulations are inevitably imperfect representations of the climate system, their behavior is relatively consistent with available comparisons. Most importantly, a key point of our study — illustrated by our simulations but not dependent upon them — is that overturning changes involving large changes in oceanic heat loss must also involve large changes in heat uptake and transport.

Finally, our results have important implications for ongoing surface climate evolution, with particular relevance to polar amplification patterns observed today: intense Arctic warming compared to more moderate Antarctic changes. Across simulated climates, the partitioning of heat, taken up in the tropics and exported towards the northern and southern polar regions, bears a close relationship with the expression of polar amplified warming in each hemisphere. Between the Cold and Warm climate simulations, the "Northern Receiving" regime, in which heat transport into the high northern latitudes intensifies, surface warming north of 60°N is three times larger than the global warming of 5.6° C; temperatures south of 60°S increase by only a factor of 1.2 (Fig. 5). In contrast, between Warm and Hot states, the "Southern Receiving" regime in which the heat transport towards Antarctica increases, high latitude warming in each hemisphere is roughly equivalent, at almost twice (1.8 times) the global mean of 4.4° C, in agreement with the hemispherically-symmetrical, polar-amplified long-term warming response to high CO_2 levels discussed by Rugenstein et al. (44). Our results imply that asynchronous polar changes are set, at least in part, by ocean dynamics through their influence on sea ice extent (53, 54), and thus high latitude radiative feedback strength (e.g. 55, 56). This evolution emphasizes that the ocean's impact on global climate evolution is likely to be state dependent. This result is important in the context of other state-dependent aspects of climate evolution, arising from "slow" earth-system dynamics (57) and "faster" climate feedbacks (58), including radiative processees (59, 60). Such components of the climate system highlight how past climate changes are imperfect proxies for those in the future. While appreciating model limitations, our results suggest that sustained future increases in radiative forcing may result in an equilibrated Southern Hemisphere warming that exceeds, relative to global mean temperature changes, what would be expected from past differences between glacial and interglacial states.

Appendix

Appendix A. Surface Transformation and overturning

Our study concerns mechanisms of deep water formation in the North Atlantic and Southern Ocean. The total formation rate of surface waters, and the relative contribution of heat and freshwater forcing components, can be calculated through the water mass transformation framework (36). Specifically, the circulation across a given density class (Ψ, Eq. 1), sustained by surface buoyancy fluxes can be quantified exactly and is referred to as the surface (water mass) transformation:

$$F(y, \sigma) = \frac{\partial}{\partial \sigma} \int_{A[\sigma' > \sigma]} f_{surf} \mathcal{H}(\sigma'(\boldsymbol{x}) - \sigma_{min}(y)) \, \mathrm{d}A \tag{5}$$

where

$$f_{surf}(x, y, t) = -\frac{\alpha}{c_p} f_H(x, y, t) - \frac{\rho_0}{\rho_{FW}} S_0 f_{FW}(x, y, t) \tag{6}$$

is the local surface buoyancy flux, α and are the coefficients of thermal and haline expansion, respectively, f_H and f_{FW} are the surface heat and freshwater fluxes, and ρ_0, ρ_{FW}, and S_0, are the reference density, freshwater density, and salinity, respectively. Also in Eq. 3, $\sigma_{min}(y)$ is the minimum density at latitude y, and A is the surface outcrop area for all densities greater that a given density, σ. Eq. 3 can be decomposed into contributions to the buoyancy flux from heat and freshwater, as shown in Fig. 3. Further, each component can be decomposed into contributions from specific processes. In Fig. 3, the contribution from sea ice formation, melt, and redistribution is presented. This calculation reveals that across all states, NADW is largely heat-driven and that elevated formation rates in both hemispheres between state are dominantly heat-driven.

Appendix B. Scaling relations

We use scaling relationships to relate the meridional heat flux in each hemisphere to climate state properties: $F_h^{\mathrm{NA}} \sim \Psi\Delta T^{\mathrm{NA}}$ and $F_h^{\mathrm{SO}} \sim WHK\Delta T^{\mathrm{SO}}/\ell$. Perturbations to the meridional heat transport, δF_h^{NA} and δF_h^{SO} about a given mean state will depend on the properties of the climate, as

$$\delta F_h^{\mathrm{NA}} = \delta\Psi(\Delta T^{\mathrm{NA}}) + \Psi(\delta\Delta T^{\mathrm{NA}}), \tag{7}$$

$$\delta F_h^{\mathrm{SO}} = \left(\delta K\frac{\Delta T^{\mathrm{SO}}}{\ell} + K\frac{\delta\Delta T^{\mathrm{SO}}}{\ell} - K\Delta T^{\mathrm{SO}}\frac{\delta\ell}{\ell^2}\right) \times WH. \tag{8}$$

Here, we keep only $\delta\Psi$ and $\delta\ell$ terms to isolate how the background state influences the relative efficiency of an adjustment in North Atlantic versus Southern Ocean dynamics, respectively, such that

$$\delta F_h^{\mathrm{NA}} \approx \Delta T^{\mathrm{NA}} \delta \Psi, \tag{9}$$

$$\delta F_h^{\mathrm{SO}} \approx -\frac{WHK\Delta T^{\mathrm{SO}}}{\ell^2} \delta \ell. \tag{10}$$

We therefore ignore perturbations in the mean temperature gradient, which assumes that they are relatively constant with climate state. Uncertainty in changes to K in the Southern Ocean are included in estimates of the effective ACC frontal length scale, ℓ (see below). We note that as $\delta\ell$ contracts, eddies may become more vigorous (50), increasing K, though this behavior also predicts a reduction in R_h in a warmer climate (Eqs. 1 and 3).

The ratio

$$\frac{\delta F_h^{\mathrm{NA}}}{\delta F_h^{\mathrm{SO}}} \sim \underbrace{\left(\frac{\Delta T^{\mathrm{NA}}}{\Delta T^{\mathrm{SO}}}\right)\left(\frac{\ell^2}{WH}\right)}_{1} \underbrace{\left(\frac{\delta \Psi}{K \delta \ell}\right)}_{2}, \tag{11}$$

then captures the relative efficiency of dynamic adjustments in either hemisphere in sustaining increased heat transport. Term 2 represents the two ocean dynamical perturbations that could adjust to accompany increased equatorial heat uptake, while term 1, R_e in Eq. 3, incorporates all aspects of the climate state that influence this efficiency (Fig. 3e).

Climate parameters ΔT^{SO} and ΔT^{NA} and ℓ are defined as follows. ΔT^{NA} diagnoses the characteristic temperature difference between the northward flowing sub-tropical surface waters and sub-polar waters in NADW formation regions. The northern boundary of the subtropical gyre is defined as the minimum in the meridional temperature gradient (in this hemisphere, temperatures generally decrease with latitude). This dynamically-defined location migrates across climate states (Fig. S7), and ΔT^{NA} differences the temperature of subtropical waters which cross this boundary, defined as the average temperatures of waters within 1° latitude to the south of this maximum in each climate. In contrast, because the region where dense NADW overflows form is largely bathymetrically constrained, we define the average temperatures of subpolar waters as those between $54-56°$N. NADW formation increases significantly in climates where heat transport into this region increases.

The diagnostic ΔT^{SO} characterizes the temperature difference across the ACC's Polar Front. As in the North Atlantic, this front shifts poleward as the climate state warms (Fig. S7). ΔT^{SO} is defined as the difference between the mean temperature of waters $\pm 1°$ latitude from the maximum in the temperature gradient, south of 50°S, corresponding to the southern boundary of the ACC. These diagnostics are representative of the robust weakening or strengthening of temperature gradients in the high latitude North Atlantic and Southern Ocean, as evident in Fig. S7. As such, qualitatively similar trends in behavior were found for various definitions and latitudes tested.

The interaction of the ACC with topographic features leads to the formation of downstream meanders, associated with a significant tightening of horizontal temperature gradients and enhanced lateral eddy fluxes (46, 47).

These meanders, as well as co-located lateral eddy heat fluxes, become more prevalent in warmer simulations (Fig. S5). To capture this intensified lateral gradient, we define the frontal length-scale as

$$\ell \equiv \frac{\Delta T^{\mathrm{SO}}}{\langle |\nabla T| \rangle}, \tag{12}$$

where ΔT^{SO} is defined above, $\langle\,\rangle$ indicates a spatial mean south of 50°S, and $|\nabla T| = \left[(\partial T/\partial x)^2 + (\partial T/\partial y)^2\right]^{1/2}$. This region is chosen to capture the increasingly efficient pathways of heat transport into the Antarctic margins; the distribution of $\Delta T^{SO}/|\nabla T|$ for this region (averaged for each ℓ) is presented in Fig. S7.

Data Archival

All simulations and source code used are publicly available at: https://doi.org/10.5281/zenodo.3976952.

Acknowledgements

This work was funded by the National Oceanic and Atmospheric Administration (NOAA) CGC Fellowship and the Natural Environment Research Council project NE/P019218/1 (E.R.N), the National Science Foundation (NSF) through grants OCE-1235488 (A.F.T.) and OCE-1559215 (J.F.A), the Packard Foundation (A.F.T.), as well as Compute Canada and the European Research Council (ERC) under the European Union's Horizon 2020 research and innovation program (grant agreement No 682602) (E.D.G.).

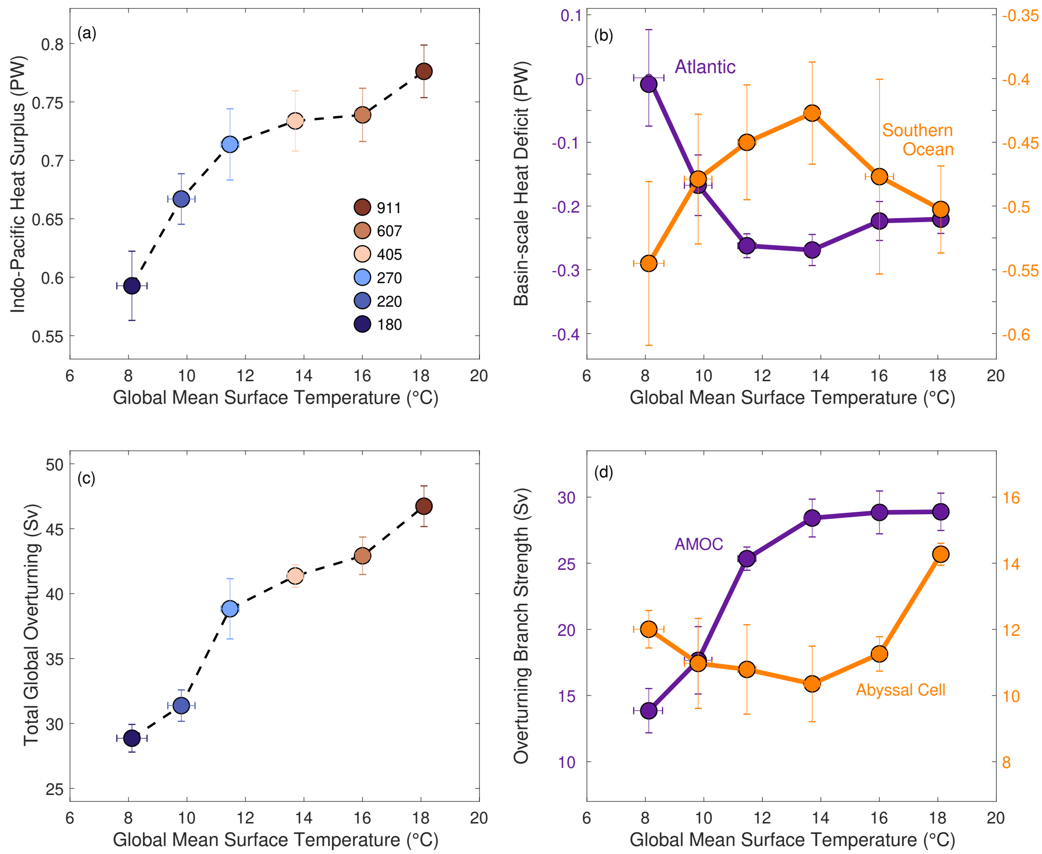

Figure 1: Basin-scale heat uptake and overturning across climate states. All panels show variations as a function of Global Mean Surface Temperature (GMST); each value is the average of four orbital configurations with the same atmospheric CO_2 levels (colored circles in panel a). Area-integrated surface heat flux (PW) over (a) Indo-Pacific (north of 30°S) and (b) Atlantic (north of 30°S and including the Arctic and marginal seas ; purple curve) and Southern Ocean (south of 30°S; orange curve); c) total global overturning (sum of the magnitude of the AMOC and abyssal branch, $\mathrm{Sv} = 10^6\ \mathrm{m}^3\ \mathrm{s}^{-1}$); d) individual magnitudes of the AMOC and abyssal overturning (see Methods). Bars represent 1 standard deviation of spread across orbital configurations (Fig. S1).

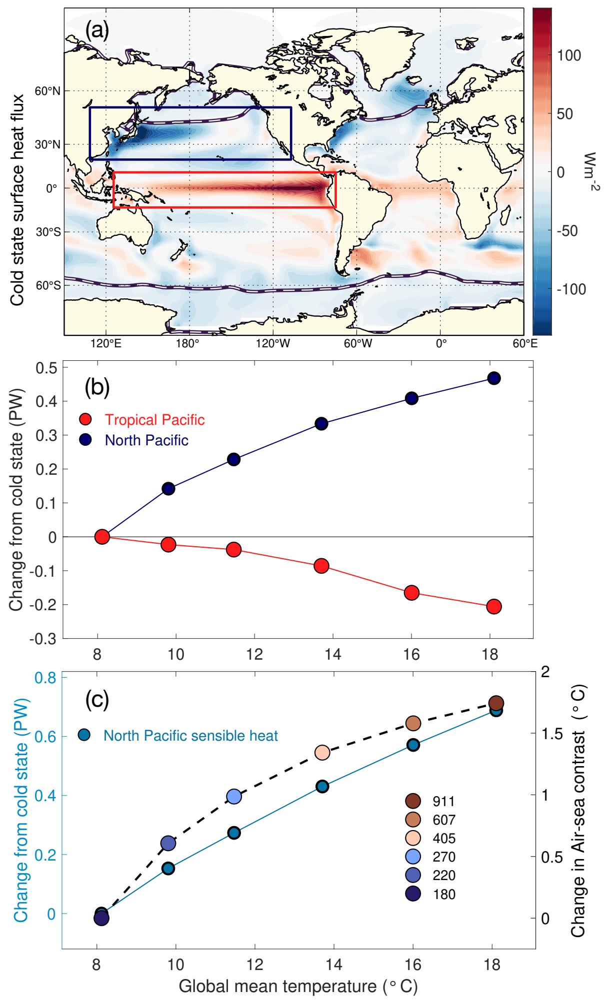

Figure 2: Summary of Indo-Pacific surface heat uptake and loss mechanisms. (a) Global distribution of surface heat flux (positive into the ocean) in the Cold state. Overlaid are the location of the 10% sea ice cover (black dashed line), the "North Pacific," which is the Indo-Pacific's primary site of heat loss (blue box), and the "Tropical Pacific," its primary site of heat uptake (red box). (b) Anomaly in total heat flux relative to the Cold state with GMST. Shown are both total Tropical Pacific heat uptake (surface heat flux summed between 10°S and 10°N, red box in panel a), shown here in red circles, and total North Pacific heat uptake (summed between 12°N and 51°N, blue box in panel a), in blue circles. Note that in all states, total North Pacific heat flux is negative; the positive anomaly shown here (blue) represents a reduction in total regional heat loss. (c) Anomaly in the North Pacific sensible heat flux (i.e., the sensible component of the total anomaly in panel b, shown here in blue circles, left axis) and the anomaly in North Pacific air-sea temperature contrast (difference between surface air temperature (SAT) and SST, here colored circles and right axis), both relative to their Cold state values, with increasing GMST. Note that sensible heat flux changes comprise the majority of the anomaly in total North Pacific heat flux in b).

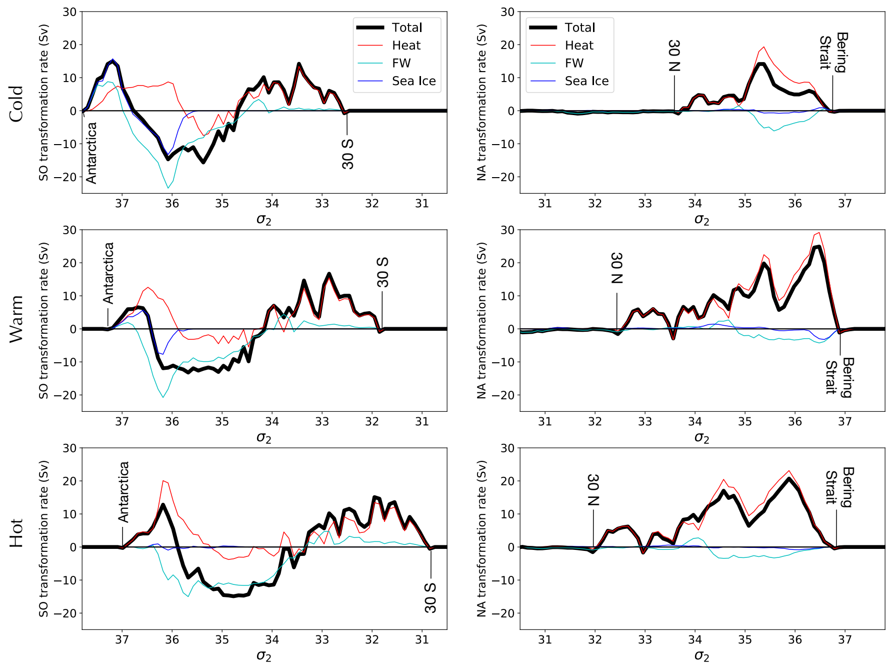

Figure 3: Surface water mass transformation (Eq. 5) in the Southern Ocean (south of 30° S, left) and North Atlantic (north of 30°N, right) in the cold (top row), warm (middle row), and hot (bottom row) climate states. Surface transformation is calculated as a function of potential density referenced to 2000 m (σ_2). The total transformation from all diabatic processes is provided in black: the sum of contributions from heat (red) and freshwater (blue). The contribution to the freshwater component specifically from sea ice formation, melt, and snow redistribution is shown in cyan. For visualization, approximate geographical boundaries are labeled. Here, positive transformation represents a volume flux towards denser classes and quantifies the role of flux components in deep water formation (see Appendix A). Note that the global ocean is less dense, on average, in warmer states, which explains the general translation of surface transformation towards lighter density classes.

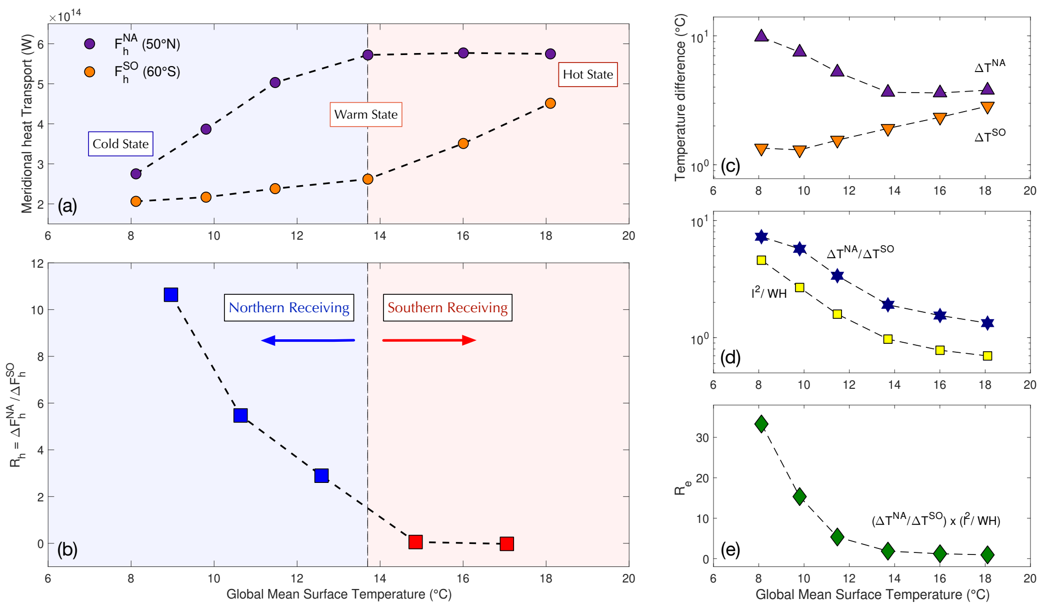

Figure 4: Characterization of meridional heat transport processes in each hemisphere across climates. a) Total meridional heat transport, MHT (PW), including parameterized cross- (GM) and along- (Redi) isopycnal eddy contributions, as diagnosed from the simulations across 50°N (purple circles) and 60°S (orange circles). b) Diagnosed ratio R_h (Eq. 1) representing how increases to MHT are partitioned between hemispheres between states, *i.e.*, $\Delta\text{MHT}_{50^\circ N}/\Delta\text{MHT}_{60^\circ S}$. c) Characteristic temperature differences across North Atlantic and Antarctic slope front (see Methods). d) Purple stars: ratio of characteristic meridional temperature contrasts in the North Atlantic and Southern Ocean with respect to GMST. Yellow squares: geometric characteristics of the ACC with GMST. Terms in (d) are multiplied to arrive (e), the ratio R_e (Eq. 3), here plotted with increasing GMST. See Appendix B and Fig. S7 for further discussions of terms.

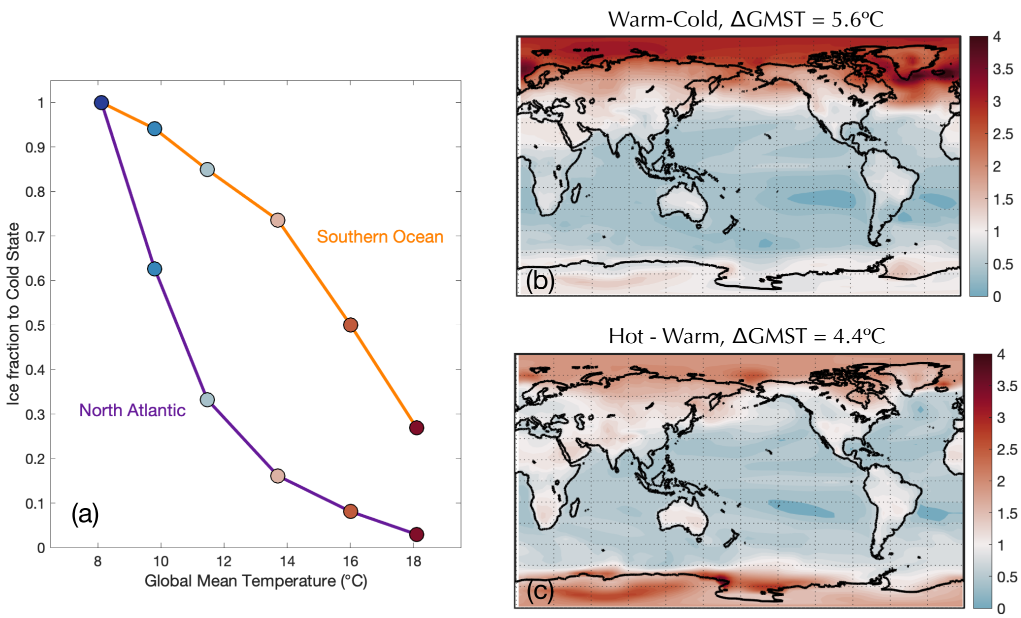

Figure 5: High-latitude characteristics across climate states. (a) Fractional Atlantic (purple) and Southern Ocean (orange) sea ice extent relative to the Cold state extent. (Right) Surface air temperature change ΔSAT($^\circ$C, color) normalized by the global mean change (ΔGMST): $\Delta\mathrm{SAT}(x, y)/\Delta\mathrm{GMST}$ for the: b) Warm - Cold states and c) Hot - Warm states. Blue [red] colors indicate where local warming is below [exceeds] global mean warming. These patterns show differences in polar amplification between states: dramatic sea ice loss and polar amplification are confined to the northern hemisphere between Cold and Warm states. Significant Antarctic declines emerge only between the Warm and Hot states.

[1] W. Broecker, The Great Ocean Conveyor, Oceanography 4 (1991) 79–89. doi:10.5670/oceanog.1991.07.

[2] K. E. Trenberth, Y. Zhang, J. T. Fasullo, L. Cheng, Observation-based estimates of global and basin ocean meridional heat transport time series, Journal of Climate 32 (2019) 4567–4583. doi:10.1175/JCLI-D-18-0872.1.

[3] A. L. Gordon, Interocean exchange of thermocline water, Journal of Geophysical Research 91 (1986) 5037–5046. doi:10.1029/jc091ic04p05037.

[4] R. Ferrari, D. Ferreira, What processes drive the ocean heat transport?, Ocean Modelling 38 (2011) 171–186. doi:10.1016/j.ocemod.2011.02.013.

[5] L. Talley, Closure of the global overturning circulation through the Indian, Pacific, and Southern Oceans: Schematics and transports, Oceanography 26 (2013) 80–97. doi:10.5670/oceanog.2011.65.

[6] E. R. Newsom, A. F. Thompson, Reassessing the Role of the Indo-Pacific in the Ocean's Global Overturning Circulation, Geophysical Research Letters 45 (2018) 422–431. doi:https://doi.org/10.1029/2018GL080350.

[7] R. M. Holmes, J. D. Zika, R. Ferrari, A. F. Thompson, E. R. Newsom, M. H. England, Atlantic Ocean Heat Transport Enabled by Indo-Pacific Heat Uptake and Mixing, Geophysical Research Letters 46 (2019) 13939–13949. doi:doi:10.1029/2019GL085160.

[8] E. A. Boyle, L. Keigwin, North Atlantic thermohaline circulation during the past 20,000 years linked to high-latitude surface temperature, Nature 330 (1987) 35–40. URL: https://doi.org/10.1038/330035a0. doi:10.1038/330035a0.

[9] W. B. Curry, D. W. Oppo, Glacial water mass geometry and the distribution of δ 13C of ΣCO2 in the western Atlantic Ocean, Paleoceanography 20 (2005) PA1017. doi:https://doi.org/10.1029/2004PA001021.

[10] J. Lynch-Stieglitz, J. F. Adkins, W. B. Curry, T. Dokken, I. R. Hall, J. C. Herguera, J. J. Hirschi, E. V. Ivanova, C. Kissel, O. Marchal, T. M. Marchitto, I. N. McCave, J. F. McManus, S. Mulitza, U. Ninnemann, F. Peeters, E. F. Yu, R. Zahn, Atlantic meridional overturning circulation during the last glacial maximum, Science 316 (2007) 66–69. doi:10.1126/science.1137127.

[11] D. C. Lund, J. F. Adkins, R. Ferrari, Abyssal Atlantic circulation during the Last Glacial Maximum: Constraining the ratio between transport and vertical mixing, Paleoceanography 26 (2011). doi:10.1029/2010PA001938.

[12] A. Burke, A. L. Stewart, J. F. Adkins, R. Ferrari, M. F. Jansen, A. F. Thompson, The glacial mid-depth radiocarbon bulge and its implications for the overturning circulation, Paleoceanography 30 (2015) 1021–1039. doi:10.1002/2015PA002778.

[13] E. Bohm, J. Lippold, M. Gutjahr, M. Frank, P. Blaser, B. Antz, J. Fohlmeister, N. Frank, M. B. Andersen, M. Deininger, Strong and deep Atlantic meridional overturning circulation during the last glacial cycle, Nature 517 (2015) 73–76. doi:10.1038/nature14059.

[14] J. R. Toggweiler, B. Samuels, Effect of drake passage on the global thermohaline circulation, Deep-Sea Research Part I 42 (1995) 477–500. doi:10.1016/0967-0637(95)00012-U.

[15] M. Nikurashin, G. Vallis, A Theory of the Interhemispheric Meridional Overturning Circulation and Associated Stratification, Journal of Physical Oceanography 42 (2012) 1652–1667. doi:10.1175/JPO-D-11-0189.1.

[16] R. Ferrari, M. F. Jansen, J. F. Adkins, A. Burke, A. L. Stewart, A. F. Thompson, Antarctic sea ice control on ocean circulation in present and glacial climates., Proceedings of the National Academy of Sciences of the United States of America 111 (2014) 8753–8758. doi:10.1073/pnas.1323922111.

[17] A. F. Thompson, A. L. Stewart, T. Bischoff, A Multibasin Residual-Mean Model for the Global Overturning Circulation, Journal of Physical Oceanography 46 (2016) 2583–2604. doi:10.1175/JPO-D-15-0204.1.

[18] M. F. Jansen, L.-P. Nadeau, The Effect of Southern Ocean Surface Buoyancy Loss on the Deep-Ocean Circulation and Stratification, Jour-

nal of Physical Oceanography 46 (2016) 3455–3470. doi:10.1175/JPO-D-16-0084.1.

[19] M. F. Jansen, L. P. Nadeau, A toy model for the response of the residual overturning circulation to surface warming, Journal of Physical Oceanography 49 (2019) 1249–1268. doi:10.1175/JPO-D-18-0187.1.

[20] M. F. Jansen, L. P. Nadeau, T. M. Merlis, Transient versus equilibrium response of the ocean's overturning circulation to warming, Journal of Climate 31 (2018) 5147–5163. doi:10.1175/JCLI-D-17-0797.1.

[21] E. Galbraith, C. de Lavergne, Response of a comprehensive climate model to a broad range of external forcings: relevance for deep ocean ventilation and the development of late Cenozoic ice ages, Climate Dynamics 52 (2019) 653–679. doi:10.1007/s00382-018-4157-8.

[22] E. D. Galbraith, E. Y. Kwon, A. Gnanadesikan, K. B. Rodgers, S. M. Griffies, D. Bianchi, J. L. Sarmiento, J. P. Dunne, J. Simeon, R. D. Slater, A. T. Wittenberg, I. M. Held, Climate variability and radiocarbon in the CM2Mc earth system model, Journal of Climate 24 (2011) 4230–4254. doi:10.1175/2011JCLI3919.1.

[23] R. Farneti, S. M. Downes, S. M. Griffies, S. J. Marsland, E. Behrens, M. Bentsen, D. Bi, A. Biastoch, C. Böning, A. Bozec, V. M. Canuto, E. Chassignet, G. Danabasoglu, S. Danilov, N. Diansky, H. Drange, P. G. Fogli, A. Gusev, R. W. Hallberg, A. Howard, M. Ilicak, T. Jung,

M. Kelley, W. G. Large, A. Leboissetier, M. Long, J. Lu, S. Masina, A. Mishra, A. Navarra, A. George Nurser, L. Patara, B. L. Samuels, D. Sidorenko, H. Tsujino, P. Uotila, Q. Wang, S. G. Yeager, An assessment of Antarctic Circumpolar Current and Southern Ocean Meridional Overturning Circulation during 1958–2007 in a suite of interannual CORE-II simulations, Ocean Modelling 93 (2015) 84–120. doi:10.1016/j.ocemod.2015.07.009.

[24] R. Bernardello, I. Marinov, J. B. Palter, J. L. Sarmiento, E. D. Galbraith, R. D. Slater, Response of the ocean natural carbon storage to projected twenty-first-century climate change, Journal of Climate 27 (2014) 2033–2053. doi:10.1175/JCLI-D-13-00343.1.

[25] W. Cheng, J. C. Chiang, D. Zhang, Atlantic meridional overturning circulation (AMOC) in CMIP5 Models: RCP and historical simulations, Journal of Climate 26 (2013) 7187–7197. doi:10.1175/JCLI-D-12-00496.1.

[26] G. Danabasoglu, P. R. Gent, Equilibrium climate sensitivity: Is it accurate to use a slab ocean model?, Journal of Climate 22 (2009) 2494–2499. doi:10.1175/2008JCLI2596.1.

[27] M. A. Rugenstein, J. Sedláček, R. Knutti, Nonlinearities in patterns of long-term ocean warming, Geophysical Research Letters 43 (2016) 3380–3388. doi:10.1002/2016GL068041.

[28] P. R. Gent, J. C. Mcwilliams, Isopycnal Mixing in Ocean Circulation Models, Journal of Physical Oceanography 20 (1990) 150–155. doi:10.1175/1520-0485(1990)020¡0150:imiocm¿2.0.co;2.

[29] C. W. Böning, A. Dispert, M. Visbeck, S. R. Rintoul, F. U. Schwarzkopf, The response of the antarctic circumpolar current to recent climate change, Nature Geoscience 1 (2008) 864–869. doi:10.1038/ngeo362.

[30] P. R. Gent, Effects of Southern Hemisphere Wind Changes on the Meridional Overturning Circulation in Ocean Models, Annual Review of Marine Science 8 (2016) 79–94. doi:10.1146/annurev-marine-122414-033929.

[31] Q. Shu, Q. Wang, Z. Song, F. Qiao, J. Zhao, M. Chu, X. Li, Assessment of Sea Ice Extent in CMIP6 With Comparison to Observations and CMIP5, Geophysical Research Letters 47 (2020) 1–9. doi:10.1029/2020GL087965.

[32] R. Seager, D. S. Battisti, J. Yin, N. Gordon, N. Naik, a. C. Clement, M. a. Cane, Is the Gulf Stream responsible for Europe's mild winters?, Quarterly Journal of the Royal Meteorological Society 128 (2002) 2563–2586. doi:10.1256/qj.01.128.

[33] S. Manabe, R. J. Stouffer, M. J. Spelman, K. Bryan, Transient responses of a coupled ocean–atmosphere model to gradual changes of atmospheric CO2. Part I: Annual mean response, J. Climate 4 (1991) 785–818.

[34] R. T. Sutton, B. Dong, J. M. Gregory, Land/sea warming ratio in response to climate change: IPCC AR4 model results and comparison with observations, Geophys. Res. Lett. 34 (2007) L02701.

[35] G. Myhre, B. H. Samset, O. Hodnebrog, T. Andrews, O. Boucher, G. Faluvegi, D. Fläschner, P. M. Forster, M. Kasoar, V. Kharin, A. Kirkevåg, J. F. Lamarque, D. Olivié, T. B. Richardson, D. Shawki, D. Shindell, K. P. Shine, C. W. Stjern, T. Takemura, A. Voulgarakis, Sensible heat has significantly affected the global hydrological cycle over the historical period, Nature Communications 9 (2018). doi:10.1038/s41467-018-04307-4.

[36] B. G. Walin, On the relation between sea-surface heat flow and thermal circulation in the ocean, Tellus 32 (1982) 187–195.

[37] S. Gu, Z. Liu, J. Zhang, J. Rempfer, F. Joos, D. W. Oppo, Coherent Response of Antarctic Intermediate Water and Atlantic Meridional Overturning Circulation During the Last Deglaciation: Reconciling Contrasting Neodymium Isotope Reconstructions From the Tropical Atlantic, Paleoceanography 32 (2017) 1036–1053. doi:10.1002/2017PA003092.

[38] J. F. Adkins, K. McIntyre, D. P. Schrag, The salinity, temperature, and δ18O of the glacial deep ocean, Science 298 (2002) 1769–1773. doi:10.1126/science.1076252.

[39] M. F. Jansen, Glacial ocean circulation and stratification explained by

reduced atmospheric temperature, Proceedings of the National Academy of Sciences 114 (2017) 45–50. doi:10.1073/pnas.1610438113.

[40] A. L. Gordon, R. F. Weiss, W. M. Smethie, M. J. Warner, Thermocline and Intermediate Water Communication Between the South Atlantic and Indian Oceans, Journal of Geophysical Research 97 (1992) 7223–7240. doi:10.1029/92JC00485.

[41] P. R. Oke, M. H. England, Oceanic response to changes in the latitude of the Southern Hemisphere subpolar westerly winds, Journal of Climate 17 (2004) 1040–1054. doi:10.1175/1520-0442(2004)017¡1040:ORTCIT¿2.0.CO;2.

[42] P. Cessi, C. S. Jones, Warm-Route versus Cold-Route Interbasin Exchange in the Meridional Overturning Circulation, Journal of Physical Oceanography 47 (2017) 1981–1997. doi:10.1175/JPO-D-16-0249.1.

[43] E. K. Schneider, Axially Symmetric Steady-State Models of the Basic State for Instability and Climate Studies. Part II. Nonlinear Calculations., Journal of Atmospheric Sciences 34 (1977) 280–296. doi:10.1175/1520-0469(1977)034¡0280:ASSSMO¿2.0.CO;2.

[44] M. Rugenstein, J. Bloch-Johnson, A. Abe-Ouchi, T. Andrews, U. Beyerle, L. Cao, T. Chadha, G. Danabasoglu, J. L. Dufresne, L. Duan, M. A. Foujols, T. Frölicher, O. Geoffroy, J. Gregory, R. Knutti, C. Li, A. Marzocchi, T. Mauritsen, M. Menary, E. Moyer, L. Nazarenko, D. Paynter,

D. Saint-Martin, G. A. Schmidt, A. Yamamoto, S. Yang, Longrunmip motivation and design for a large collection of millennial-length AOGCM simulations, Bulletin of the American Meteorological Society 100 (2019) 2551–2569. doi:10.1175/BAMS-D-19-0068.1.

[45] A. Yamamoto, A. Abe-Ouchi, M. Shigemitsu, A. Oka, K. Takahashi, R. Ohgaito, Y. Yamanaka, Global deep ocean oxygenation by enhanced ventilation in the Southern Ocean under long-term global warming, Global Biogeochemical Cycles 29 (2015) 1801–1815. doi:https://doi.org/10.1002/2015GB005181.

[46] A. F. Thompson, A. C. Naveira Garabato, Equilibration of the Antarctic Circumpolar Current by Standing Meanders, Journal of Physical Oceanography 44 (2014) 1811–1828. doi:10.1175/JPO-D-13-0163.1.

[47] C. O. Dufour, S. M. Griffies, G. F. de Souza, I. Frenger, A. K. Morrison, J. B. Palter, J. L. Sarmiento, E. D. Galbraith, J. P. Dunne, W. G. Anderson, R. D. Slater, Role of Mesoscale Eddies in Cross-Frontal Transport of Heat and Biogeochemical Tracers in the Southern Ocean, Journal of Physical Oceanography 45 (2015) 3057–3081. doi:10.1175/JPO-D-14-0240.1.

[48] S. R. Jayne, J. Marotzke, The oceanic eddy heat transport, Journal of Physical Oceanography 32 (2002) 3328–3345. doi:10.1175/1520-0485(2002)032¡3328:TOEHT¿2.0.CO;2.

[49] J. Marshall, K. Speer, Closure of the meridional overturning circulation through Southern Ocean upwelling, Nature Geoscience 5 (2012) 171–180. doi:10.1038/ngeo1391.

[50] R. Abernathey, J. Marshall, D. Ferreira, The Dependence of Southern Ocean Meridional Overturning on Wind Stress, Journal of Physical Oceanography 41 (2011) 2261–2278. doi:10.1175/JPO-D-11-023.1.

[51] M. Latif, T. P. Barnett, Decadal climate variability over the North Pacific and North America: Dynamics and predictability, Journal of Climate 9 (1996) 2407–2423. doi:https://doi.org/10.1175/1520-0442(1996)009¡2407:DCVOTN¿2.0.CO;2.

[52] R. J. Stouffer, S. Manabe, Equilibrium response of thermohaline circulation to large changes in atmospheric CO2 concentration, Climate Dynamics 20 (2003) 759–773. doi:10.1007/s00382-002-0302-4.

[53] C. M. Bitz, M. M. Holland, E. C. Hunke, R. Moritz, Maintenance of the Sea-Ice Edge, Journal of Climate (2005) 2903–2921.

[54] B. E. J. Rose, J. Marshall, Ocean Heat Transport, Sea Ice, and Multiple Climate States: Insights from Energy Balance Models, Journal of the Atmospheric Sciences 66 (2009) 2828–2843. doi:10.1175/2009JAS3039.1.

[55] H. A. Singh, P. J. Rasch, B. E. J. Rose, Increased Ocean Heat Convergence Into the High Latitudes With CO2 Doubling Enhances Polar-

Amplified Warming, Geophysical Research Letters 44 (2017) 510–583. doi:https://doi.org/10.1002/2017GL074561.

[56] M. F. Stuecker, C. M. Bitz, K. C. Armour, C. Proistosescu, S. M. Kang, S. P. Xie, D. Kim, S. McGregor, W. Zhang, S. Zhao, W. Cai, Y. Dong, F. F. Jin, Polar amplification dominated by local forcing and feedbacks, Nature Climate Change 8 (2018) 1076–1081. doi:10.1038/s41558-018-0339-y.

[57] R. Caballero, M. Huber, State-dependent climate sensitivity in past warm climates and its implications for future climate projections, Proceedings of the National Academy of Sciences of the United States of America 110 (2013) 14162–14167. doi:10.1073/pnas.1303365110.

[58] A. S. Von Der Heydt, P. Köhler, R. S. Van De Wal, H. A. Dijkstra, On the state dependency of fast feedback processes in (paleo) climate sensitivity, Geophysical Research Letters 41 (2014) 6484–6492. doi:10.1002/2014GL061121.

[59] T. Friedrich, A. Timmermann, M. Tigchelaar, O. E. Timm, A. Ganopolski, Nonlinear climate sensitivity and its implications for future greenhouse warming, Science Advances 2 (2016). doi:10.1126/sciadv.1501923.

[60] J. Bjordal, T. Storelvmo, K. Alterskjær, T. Carlsen, Equilibrium climate sensitivity above 5 °C plausible due to state-dependent cloud feedback, Nature Geoscience 13 (2020) 718–721. doi:10.1038/s41561-020-00649-1.

Declaration of interests

☒ The authors declare that they have no known competing financial interests or personal relationships that could have appeared to influence the work reported in this paper.

☐The authors declare the following financial interests/personal relationships which may be considered as potential competing interests:

Declaration of author contributions

Emily Newsom led in designing the study, analyzing the results, and writing the manuscript.

Andrew Thompson contributed to the study design, analysis, and manuscript writing.

Jess Adkins contributed to the study design, analysis and edited the manuscript

Eric Galbraith performed the numerical simulations, interpretation of results, and edited the manuscript.

Highlights

- Total ocean heat uptake over the Indo-Pacific increases monotonically in warmer climate states.
- Cooling from Atlantic and Southern polar regions increases asymmetrically with climate warming.
- Reconfigurations in heat-driven global ocean overturning evolve with polar cooling changes.
- Polar-amplified warming accompanies asymmetric overturning changes in each hemisphere.